AGU PUBLICATIONS

JGR

Journal of Geophysical Research: Atmospheres

RESEARCH ARTICLE
10.1002/2014JD022481

Key Points:
- We developed an algorithm for retrieving emissivity and temperature of sea ice
- Retrieved sea ice emissivities are in good agreement with theoretical as well as in situ values
- Potential applications for studying climate changes associated with sea ice

Supporting Information:
- Readme
- Text S1
- Text S2

Correspondence to:
B.-J. Sohn,
sohn@snu.ac.kr

Citation:
Lee, S.-M., and B.-J. Sohn (2015), Retrieving the refractive index, emissivity, and surface temperature of polar sea ice from 6.9 GHz microwave measurements: A theoretical development, *J. Geophys. Res. Atmos.*, *120*, 2293–2305, doi:10.1002/2014JD022481.

Received 25 AUG 2014
Accepted 17 FEB 2015
Accepted article online 20 FEB 2015
Published online 26 MAR 2015

Retrieving the refractive index, emissivity, and surface temperature of polar sea ice from 6.9 GHz microwave measurements: A theoretical development

Sang-Moo Lee[1] and Byung-Ju Sohn[1]

[1]School of Earth and Environmental Sciences, Seoul National University, Seoul, South Korea

Abstract A new method for retrieving the refractive index, horizontally and vertically polarized emissivities (ε_H, ε_V), and temperature of sea ice has been developed by using the "combined Fresnel equation," which combines two Fresnel-polarized reflectivity equations into one. By using low-frequency 6.9 GHz brightness temperature measurements, the full microwave radiative transfer equation was simplified so that the atmospheric influence on the horizontally and vertically polarized brightness temperatures (T_H, T_V) can be ignored, and thus $\varepsilon_H/\varepsilon_V = T_H/T_V$. Since ε_H can be expressed by ε_V according to the combined Fresnel equation (or vice versa), ε_H and ε_V can directly be retrieved from T_H/T_V. The Advanced Microwave Scanning Radiometer–Earth Observing System (AMSR-E) measurements based on the developed method indicate that retrieved ε_V is close to 1, regardless of region and season, which is consistent with the theoretically expected value of ε_V near the Brewster angle (close to AMSR-E viewing angle of 55°). This finding strongly suggests that ε_H and ε_V hold the same degree of accuracy because $\varepsilon_H/\varepsilon_V = T_H/T_V$. Such expected accuracy can also be applied to associated sea ice temperature and refractive index retrievals. Likewise, the close agreement of retrieved sea ice temperature with in situ measurement at the ice surface suggests that emissivity and refractive index retrievals are also sound. Some caveats of this approach for the surface temperature over the area including open water are discussed.

1. Introduction

Sea ice, or frozen seawater found in polar regions, has been recognized as one of the most important variables influencing the contemporary Earth's climate [*Stocker et al.*, 2013]. The large spatial coverage of sea ice area occupies 5–8% of the total area of the global ocean, and the associated high albedo can effectively prohibit heat and momentum exchanges between the atmosphere and ocean [*Comiso et al.*, 2003; *Hall et al.*, 2004]. Thus, any change in sea ice extent implies a change in the energy budget that can directly influence global climate [*Flanner et al.*, 2011]. Therefore, it is critical to observe and monitor various parameters related to sea ice, from which its climate implications can be examined. However, because of the extreme climate conditions over the polar region, direct observation of sea ice parameters is difficult and measurements are limited within local areas or short observation periods.

In order to circumvent the limitations associated with difficult direct measurement, remote sensing tools are often used. In particular, satellite remote sensing techniques have become more powerful and popular with the advent of satellite technology. Visible/infrared (VIS/IR) measurements have been frequently used to provide rich information on the sea ice with high spatial resolution [*Hall et al.*, 2004; *Key et al.*, 2013]. But, VIS measurement is only possible during the summer months, and frequent cloud occurrence over the polar region hampers continuous and stable retrieval. IR techniques may add more information, particularly during the winter; however, low cloud top temperatures are not easily discernible from the sea ice temperatures [*Ackerman*, 1996; *Liu et al.*, 2004; *Bromwich et al.*, 2012], yielding erroneous results. Thus, VIS/IR measurements are difficult to use for producing spatially and temporally continuous sea ice data.

Unlike VIS/IR radiation, emitted microwave (MW) radiation from the surface can transmit through nonprecipitating clouds, allowing satellites to detect sea ice conditions even in the presence of clouds. However, MW spatial resolution is much coarser compared to VIS/IR observations, providing limited information for studying detailed dynamics and physics related to sea ice change. Nevertheless, a majority of broad and consistent

global sea ice data have been obtained from MW measurements [*Gloersen et al*., 1992; *Comiso et al*., 2003; *Peng et al*., 2013]. Despite the success of MW measurements for the retrieval of sea ice parameters, their application has been limited to parameters such as sea ice concentration and snow depth [*Comiso et al*., 1997; *Markus and Cavalieri*, 2000; *Comiso et al*., 2003; *Markus et al*., 2006; *Key et al*., 2013; *Zhang et al*., 2013]. Although these parameters are important for understanding sea ice influences on global climate, other elementary parameters such as sea ice temperature, emissivity, and refractive index are also much needed.

In general, the retrieval of sea ice emissivity from MW measurements is largely based on the sea ice temperature information obtained from IR measurements [*Comiso*, 1983; *Hall et al*., 2004] or from in situ measurements combined with radiative transfer modeling [*Hewison and English*, 1999; *Haggerty and Curry*, 2001; *Mathew et al*., 2008; *Hwang and Barber*, 2008]. However, sea ice emissivity from MW measurements with an aid of IR-based surface temperatures contains potentially serious errors. This is because the sea ice temperature from MW measurements is an integrated temperature of the emitting layer containing sea ice as well as snow, which is equivalent to the physical temperature of the sea ice-emitting layer associated with the penetration depth. The penetration depth is determined by the imaginary part of refractive index, which is affected by salinity and snow/ice metamorphism [*Ulaby et al*., 1984, 1986; *Rosenfeld and Grody*, 2000]. The penetration depth of sea ice is about 7.5 cm for first-year ice and 30 cm for multiyear ice at 6.925 GHz [*Mathew et al*., 2009, Table 2]. It is also noted that a snow layer is nearly transparent, but it is considered to be a part of the emitting layer if snow exists above the ice. Thus, the temperature within the penetration depth may be considered to be a representing temperature of the emitting layer [*Hwang and Barber*, 2008; *Mathew et al*., 2008, 2009]. On the other hand, the surface temperature sensed by IR measurements represents only the skin temperature of the ice or snow surface. Therefore, when emissivity obtained from IR-based surface temperatures is used as input for the ice temperature retrieval from MW measurements, the results are often erroneous because of the different representation of the emitting layer. Thus, the direct retrieval of surface emissivity from MW-based satellite measurements should be beneficial as it allows for the estimation of the physical temperature of sea ice or snow.

In this study, we attempt to retrieve sea ice parameters, such as physical temperature, emissivity, and refractive index from MW measurements, using 6.925 GHz brightness temperature. For that objective, we use the "combined Fresnel equation" that was analytically derived by *Sohn and Lee* [2013], in which one component of polarized reflectivity in the Fresnel equations can be expressed by the other component of polarized reflectivity or vice versa. In this paper, we will demonstrate that the derived sea ice parameters are consistent with theoretically expected values as well as with in situ measurements, and further suggest that the retrieved data can be used for examining climate change studies particularly those associated with sea ice changes.

2. Theoretical Background and Algorithm

In the satellite MW remote sensing, the radiative transfer equation at a given frequency (ν) and polarization state (p) with nonscattering conditions can be expressed as [*Liou*, 2002]

$$T_p(\nu) = \varepsilon_p(\nu) T_s e^{-\tau} + T_{p,\mathrm{up}}(\nu) + \left(1 - \varepsilon_p(\nu)\right) T_{p,\mathrm{down}}(\nu) \tag{1}$$

where $T_p(\nu)$ is the polarized brightness temperature from satellite MW measurements, $\varepsilon_p(\nu)$ and T_s are the polarized emissivity and temperature of the emitting layer, respectively, τ is the atmospheric optical thickness from the surface to the sensor, and $T_{p,\mathrm{up}}(\nu)$ and $T_{p,\mathrm{down}}(\nu)$ are the vertically integrated atmospheric upwelling and downwelling brightness temperatures, respectively.

In the MW low-frequency spectral window channels such as 6.925 GHz of the Advanced Microwave Scanning Radiometer–Earth Observing System (AMSR-E), the atmospheric contribution is assumed to be negligible over ice/snow surfaces if there are no precipitating clouds [*Haggerty and Curry*, 2001; *Njoku et al*., 2003]. Under this assumption, equation (1) can be approximated by

$$T_V(\nu) = \varepsilon_V(\nu) T_s \tag{2}$$

$$T_H(\nu) = \varepsilon_H(\nu) T_s \tag{3}$$

where subscripts V and H represent vertically and horizontally polarized components, respectively. From equations (2) and (3), the ratio between polarized emissivities can be expressed by the ratio of measured polarized brightness temperatures, i.e.,

$$\frac{\varepsilon_V(v)}{\varepsilon_H(v)} = \frac{T_V(v)}{T_H(v)} \tag{4}$$

Equation (4) suggests that there seems to be no way to directly measure two polarized emissivities from satellite-measured polarized brightness temperatures without a priori information about one of the two polarized components of the emissivity. Furthermore, since emissivity is a function of the satellite viewing angle [*Mathew et al*., 2008], problems become more difficult for cross-tracking MW radiometers such as the Advanced Microwave Sounding Unit (AMSU) sensor. We propose a new method to retrieve surface emissivities (and thus physical surface temperature) from two measured polarized brightness temperatures without a priori information by using the combined Fresnel equation analytically derived by *Sohn and Lee* [2013]. Here we briefly introduce the methodology.

2.1. Combined Fresnel Equation

Over a smooth surface assuming an incident electromagnetic wave with fixed phase, polarization reflection follows Fresnel's reflection theory [*Liou*, 2002], i.e.,

$$R_V(v) = \left| \frac{N_r^2 \cos\theta - \sqrt{N_r^2 - \sin^2\theta}}{N_r^2 \cos\theta + \sqrt{N_r^2 - \sin^2\theta}} \right|^2 \tag{5}$$

$$R_H(v) = \left| \frac{\cos\theta - \sqrt{N_r^2 - \sin^2\theta}}{\cos\theta + \sqrt{N_r^2 - \sin^2\theta}} \right|^2 \tag{6}$$

where $R_V(v)$ and $R_H(v)$ are the vertically and horizontally polarized surface reflectivities, respectively, θ is the incident angle (or satellite viewing angle), and N_r is the adjusted real refractive index, which can be expressed by

$$N_r = \frac{\sqrt{2}}{2} \left\{ n_r^2 - n_i^2 + \sin^2\theta + \left[\left(n_r^2 - n_i^2 - \sin^2\theta \right)^2 + 4 n_r^2 n_i^2 \right]^{1/2} \right\}^{1/2} \tag{7}$$

where n_r and n_i are the real and imaginary parts of the relative refractive index, respectively.

It is difficult to solve equations (5) and (6) because a priori refractive indices are required. The difficulty may be avoided when an analytical relationship between two Fresnel-polarized reflectivities (i.e., combined Fresnel equation) is employed, as in *Sohn and Lee* [2013], i.e.,

$$R_V(v) = R_H(v)^2 \left(\frac{1 + R_H(v)^{-1/2} \cos 2\theta}{1 + R_H(v)^{1/2} \cos 2\theta} \right)^2 = f(R_H(v), \theta) \tag{8}$$

where f represents an analytical function. Equation (8) shows that one component of polarized reflectivity can be expressed as a function of the other component of polarized reflectivity or vice versa, for a given incident angle. It is now possible to solve equation (4) without a priori information on refractive index from satellite-measured polarized brightness temperatures (i.e., T_V and T_H) because of the relationship interlinked between two reflectivities as shown in equation (8).

In order to apply the combined Fresnel equation, a smooth ice surface condition is assumed. In the case of a rough surface, however, scattered or diffused radiation can impinge on specular angles of reflection, causing difficulty in its application. To investigate the effect of surface roughness on the retrieved parameter (for example emissivity), a sensitivity test is taken using a roughness model of the Bragg scattering for determining the surface emissivity in the microwave spectrum [*Wu and Fung*, 1972; *Choudhury et al*., 1979; *English and Hewison*, 1998]. In the Bragg scattering model [*Choudhury et al*., 1979], the rough surface polarized emissivity ($\overline{\varepsilon_p}$) at the viewing angle θ can be expressed as follows:

$$\overline{\varepsilon_p} = 1 - R_p \exp\left[-\left(\frac{4\pi\sigma \cos\theta}{\lambda} \right)^2 \right] \tag{9}$$

Table 1. Horizontally and Vertically Polarized Emissivity at 6 GHz for Specular/Rough Ice, Dry Snow, Moist Snow, and Wet Snow Surfaces Calculated From the Bragg Scattering Model [*Choudhury et al.*, 1979] With Different RMS Heights at an Incident Angle of 55°

	Small-Scale Roughness (σ in mm)						
	specular	$\sigma = 0.1$	$\sigma = 0.2$	$\sigma = 0.5$	$\sigma = 1.0$	$\sigma = 2.0$	$\sigma = 3.0$
$\varepsilon_{ice,H}$	0.7812	0.7812	0.7813	0.7823	0.7856	0.7958	0.8083
$\varepsilon_{snow,H}$	0.9994	0.9994	0.9994	0.9994	0.9994	0.9994	0.9995
$\varepsilon_{moist\text{-}snow,H}$	0.9792	0.9792	0.9792	0.9793	0.9796	0.9810	0.9827
$\varepsilon_{wet\text{-}snow,H}$	0.8178	0.8178	0.8179	0.8187	0.8215	0.8232	0.8378
$\varepsilon_{ice,V}$	0.9951	0.9951	0.9951	0.9951	0.9952	0.9954	0.9959
$\varepsilon_{snow,V}$	0.9999	0.9999	0.9999	0.9999	0.9999	0.9999	0.9999
$\varepsilon_{moist\text{-}snow,V}$	0.9991	0.9991	0.9991	0.9991	0.9991	0.9991	0.9992
$\varepsilon_{wet\text{-}snow,V}$	0.9982	0.9982	0.9982	0.9982	0.9982	0.9983	0.9985

where σ (so-called small-scale roughness) is the root-mean-square (RMS) height of the surface, and λ is the wavelength.

The rough surface emissivity for 6 GHz at AMSR-E viewing zenith angle of 55° is calculated for both specular and rough surface of ice and snow with N_r for ice and snow [*Sadiku*, 1985] and σ values from 0 to 3 mm as inputs to the Bragg scattering model of equation (9). Sensitivity results are provided in Table 1. As the surface roughness increases, the difference between specular and rough surface emissivities becomes larger. In *English and Hewison* [1998] and *Hewison and English* [1999], the RMS height of sea ice and snow smaller than 0.2 mm was used for calculating the surface emissivities. Other studies showed that an RMS height of sea ice is between 0.25 mm and 2.5 mm [*Mai et al.*, 1996; *Manninen*, 1997; *Wen et al.*, 2011]. Even though σ becomes large, up to 3 mm, however, it gives rise to at most 3.5% error in horizontally polarized emissivity and near-zero change in vertically polarized emissivity, in comparison to the corresponding emissivities from the specular surface. Furthermore, the roughness effect appears to be negligible at the satellite observation scale except in extreme relief such as mountainous terrain [*De Jeu*, 2003]. It also has been reported that the surface roughness effect on the emissivity in microwave low frequencies such as C band (i.e., 4–8 GHz) is minimal in particular at the viewing angles between 20° and 60° [*Ulander et al.*, 1992; *Girard and Girard*, 2003; *Chassignet and Verron*, 2006]. Therefore, in this study, sea ice surface is considered to be smooth enough to apply the combined Fresnel equation for retrieving sea ice properties from MW measurements.

2.2. Retrieval Algorithm for Surface Emissivity and Physical Temperature

In the MW spectral range, the physical emissivity can be defined as an integrated value representing the emitting layer within the penetration depth [*Hall et al.*, 2004; *Markus et al.*, 2006; *Hwang and Barber*, 2008]. Since the physical emissivity $\varepsilon_p(v)$ can be expressed as $1 - R_p(v)$, the following equation is obtained after combining equation (4) with equation (8):

$$\frac{1 - R_H(v)}{1 - R_V(v)} = \frac{1 - R_H(v)}{1 - f(R_H(v))} = \frac{T_H(v)}{T_V(v)} \tag{10}$$

Equation (10) becomes identical to equation (4). Since $T_V(v)$ and $T_H(v)$ are satellite-measured brightness temperatures at a given viewing angle θ, horizontally (and/or vertically) polarized reflectivity can be estimated without a priori information on the refractive index of the emitting layer. Then it is straightforward to estimate the physical temperature of the emitting layer using equations (2) and (3).

Also noted in *Sohn and Lee* [2013] is the relationship between the adjusted real refractive index and one component of reflectivity (the N_r-R_H relationship):

$$N_r^2 = 1 + \frac{4R_H^{1/2}\cos^2\theta}{\left(R_H^{1/2} - 1\right)^2} \tag{11}$$

Thus, the adjusted real refractive index (N_r) can be measured from the polarized component of brightness temperature and satellite viewing angle. Since the real component of refractive index is much larger than

the imaginary component [*Sadiku*, 1985; *Mätzler and Wegmüller*, 1987; *Warren and Brandt*, 2008], the real component of the adjusted refractive index (N_r) for the polar sea ice should be nearly equal to the real component of the refractive index (n_r), as expressed in equation (7). Because of this reason, the retrieved N_r is considered to be the proxy refractive index.

3. Data Used

For testing the algorithm described in section 2, we use MW brightness temperatures measured from AMSR-E on board the Aqua satellite. AMSR-E is a conical scanning MW radiometer, measuring horizontally and vertically polarized brightness temperatures at 6.925, 10.65, 18.7, 23.8, 36.5, and 89.0 GHz. The spatial sampling resolution varies from 43 km × 75 km for 6.925 GHz to 3.7 km × 6.5 km for 89.0 GHz [*Kawanishi et al*., 2003; *Li et al*., 2004]. In this study, level 3 monthly ascending/descending brightness temperatures at 6.925 GHz (hereafter 6.9 GHz) and sea ice concentration for January 2010 and July 2010 are used. These level 3 data are available at each 25 km × 25 km grid. The AMSR-E sea ice concentration is based on the bootstrap algorithm developed by *Comiso et al*. [2003]. These data were downloaded from the Global Change Observation Mission (GCOM) website (http://gcom-w1.jaxa.jp/). The algorithm is applied to monthly mean bright temperatures obtained by taking an average of temperatures in both ascending and descending nodes if the corresponding sea ice concentrations from both bright temperatures are greater than 95%.

For validating the algorithm, we compare the daily satellite-retrieved temperature with the U.S. Army Cold Regions Research and Engineering Laboratory (CRREL) ice mass balance (IMB) buoy data [*Polashenski et al*., 2011]. The CRREL IMB data used in this study consist of air temperature at 1.5 m above the ice surface, ice temperature from the ice surface to the bottom with a 10 cm depth interval, and snow depth above the ice. Daily averages were from snow/ice data taken at every 2 h and hourly based surface air temperature, which were downloaded from the CRREL website (http://imb.erdc.dren.mil/). IMB data collected over the Beaufort Sea during 1 January 2007 to 30 April 2007 are used for validating the temperature retrieval algorithm.

In order to compare with CRREL IMB data on the daily basis, we use AMSR-E data level 3 daily averaged ascending/descending brightness temperatures at 6.9 GHz in a spatial resolution of 25 km × 25 km. Daily mean AMSR ice temperature is obtained by taking a simple average of ice temperatures retrieved from daily mean ascending/descending brightness temperatures. In addition, daily mean sea ice concentrations based on the bootstrap algorithm are also downloaded from the GCOM website.

4. Results

4.1. Proxy Refractive Index

Figure 1 shows the spatial distributions of N_r at 6.9 GHz in January and July 2010 for both the Arctic and Antarctic. The Arctic sea ice shows larger regional variation of N_r in January compared to the winter distribution of the sea ice over the Antarctic. Most of the region shows N_r smaller than 1.40, but slightly larger values occur in the area east of Greenland toward the Chuckchi Sea, as well as the area along the sea ice edge. Exceptionally larger values are found in the Bering Sea, in which newly formed ice is abundant, including thin ice. Larger values are likely due to the open water influence on the N_r. This is the area showing AMSR-E-derived sea ice concentration $>$95% and where the AMSR-E product might be less accurate in this region [*Cavalieri et al*., 2006]. Furthermore, error may be due to the temperature dependence of emissivity and its impact on the sea ice determination over this newly formed thin sea ice area [*Hwang et al*., 2008]. The overall mean value of N_r in January over the entire ice area over the Arctic is about 1.39.

During the boreal summer (July), the much reduced sea ice area, concentrated over the North Pole region, shows generally larger N_r compared to the winter distribution (January). The July average of 1.51 for overall N_r is larger than the average for January 2010. The theoretically calculated N_r using the refractive index data by *Sadiku* [1985] for pure ice, dry snow, moist snow, and wet snow at 6.9 GHz are 1.78, 1.02, 1.12, and 1.65, respectively. Considering that the emitting layer of MW radiation generally includes the snowpack above the ice, the retrieved N_r value should occur between the sea ice and snow values as expected from refractive index values varying with snow condition [*Sadiku*, 1985]. Since snow above the sea ice during the winter is likely drier than that during the summer, a relatively larger N_r can be expected for July because the real

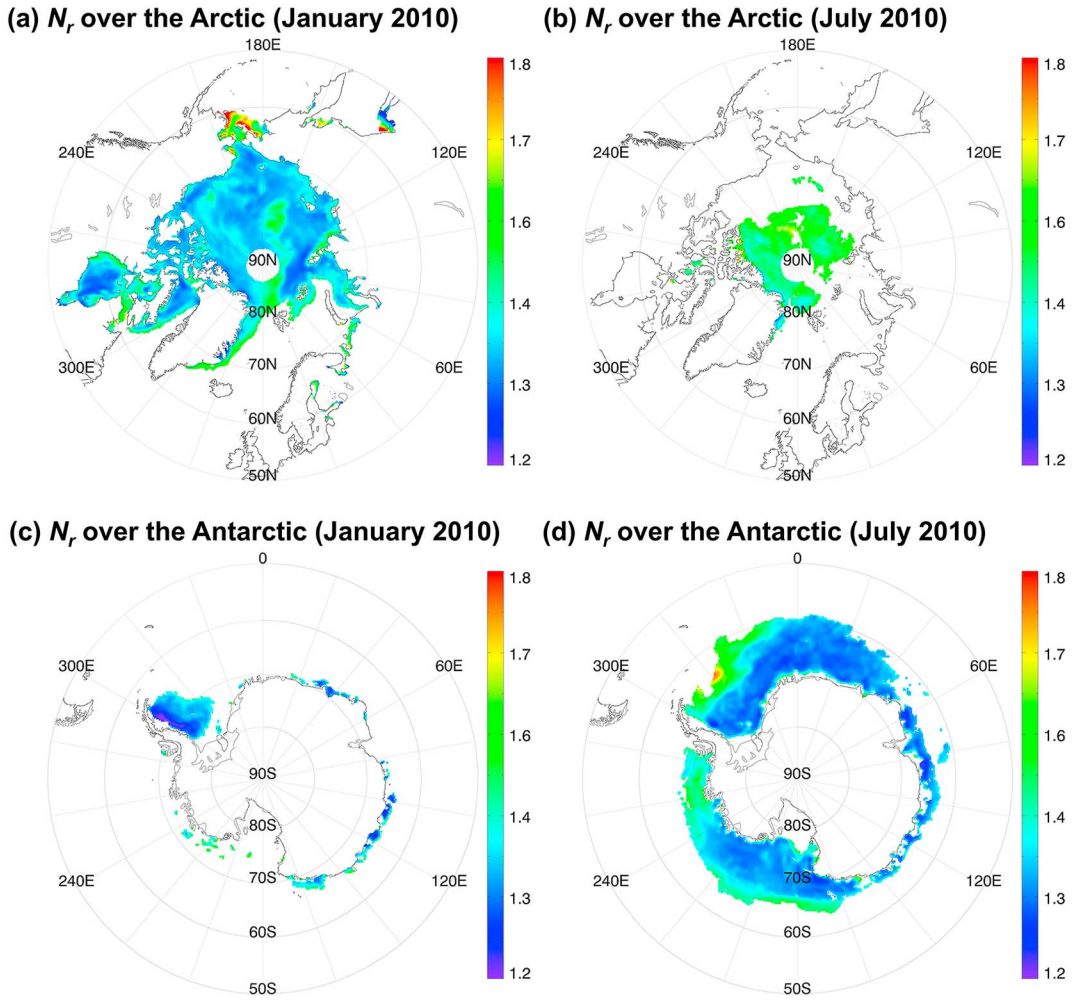

Figure 1. Retrieved refractive index of sea ice in (top) the Arctic and (bottom) the Antarctic Oceans. (a and c) For January 2010. (b and d) For July 2010.

component of the refractive index for the moist and wet snow is larger than for dry snow. This expectation based on snow wetness is consistent with the overall averages of N_r during the winter and summer, i.e., 1.39 versus 1.51.

Over the ocean surrounding Antarctica, the mean values of N_r are around 1.35 in January and 1.36 in July, which are also in the expected range of values. However, compared to the difference found for the Arctic, the difference between N_r in summer and in winter is considerably smaller. The highest N_r in winter (July) is located over the northeastern Weddell Sea. Considering that the Brazil warm current influences this area, a plentiful amount of wet or watery snow can be expected, causing larger values of N_r. However, it is surprising to note the smaller value of N_r during the summer (January) in the western Weddell Sea.

One may suspect that regional and seasonal differences in N_r are also controlled by the changes in sea ice salinity. In fact, n_i is strongly affected by the ice salinity. Generally, n_i for the first-year ice is 3 to 10 times larger than for multiyear ice because the salinity of the first-year sea ice is about 5 times larger [*Ulaby et al.*, 1986]. However, the salinity effect on N_r should be very small because the magnitude of n_i is in the 10^{-2} to 10^{-5} order of n_r [*Sadiku*, 1985], implying that the salinity effect should not be a cause of inducing such difference.

4.2. Horizontally/Vertically Polarized Emissivities (ε_H, ε_V)

Polarized emissivities of sea ice representing the emitting layer can be estimated from the ratio of polarized brightness temperatures as given in equation (10). Spatial distributions of the retrieved polarized emissivities

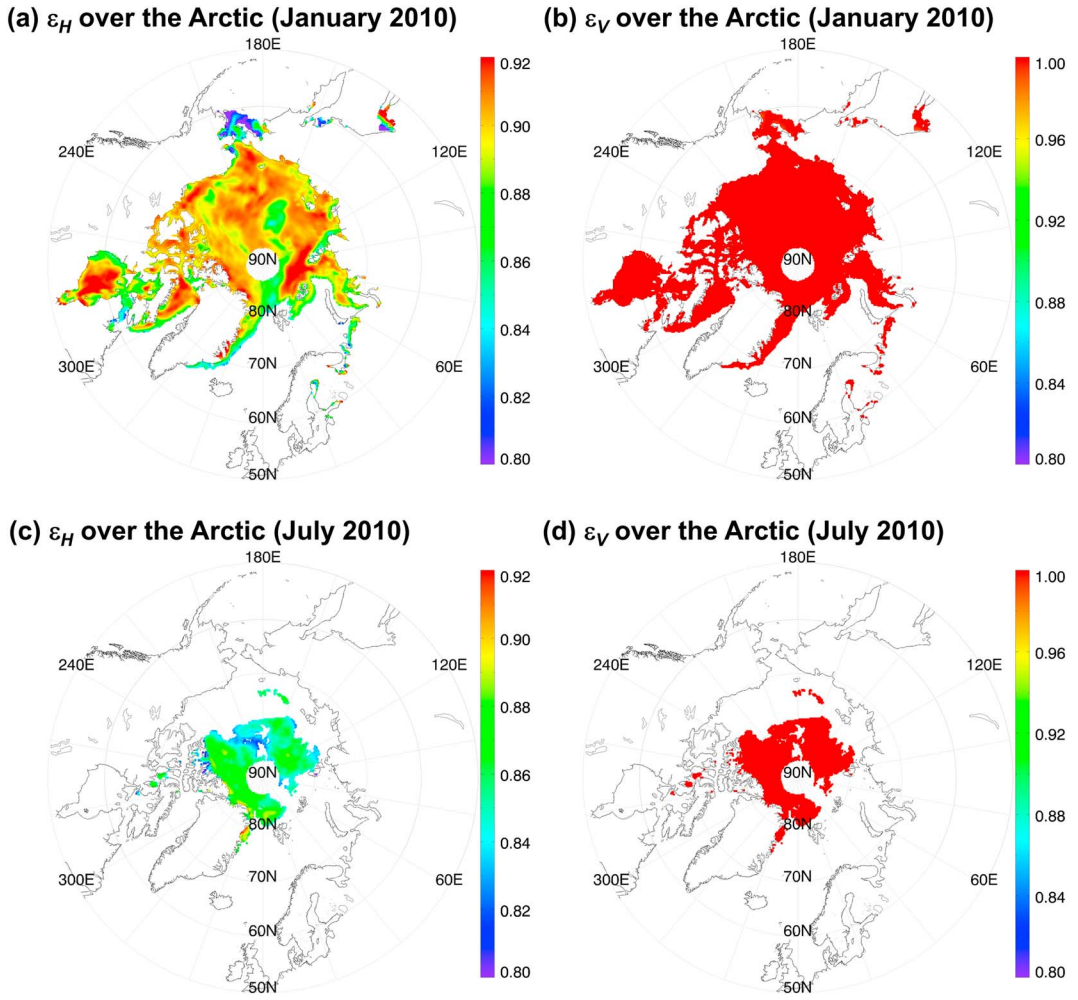

Figure 2. Retrieved (left) horizontally and (right) vertically polarized emissivities for the Arctic sea ice for (top) January and (bottom) July 2010.

at the AMSR-E viewing angle (i.e., 55°) for the Arctic and the Antarctic are shown in Figures 2 and 3, respectively. More complex distributions of ε_H are noted in the Arctic. Lower ε_H values are found in the area extending from the east of Greenland to the East Siberian Sea through the eastern part of the North Pole region. Other lower ε_H areas are also found near the coasts of Hudson Bay and the Baffin Islands, as well as the area from the north land islands to the Laptev Sea (located north of Taymir Peninsula, Russia). The lowest ε_H areas are found in the Bering Sea, which again is likely influenced by open waters caused by erroneous sea ice concentration data. Overall, the mean value of ε_H during January 2010 over the Arctic is 0.89, while the ε_V in the same winter month is found to be nearly 1 (0.997).

During July in the Arctic, ε_H is smaller than 0.90, with the lowest areas found near Makarov Basin (~82°N) showing values around 0.82. The overall July average of ε_H is approximately 0.86. Generally, lower ε_H during the summer is also influenced by open water within the sea ice area. Again, the ε_V during the summer is nearly 1.

In contrast to the Arctic region, ε_H over the Antarctic appears much simpler in terms of spatial homogeneity (Figure 3). Higher values above 0.90 in the winter are found around the oceans surrounding Antarctica, except for north of the Weddell and Bellingshausen Seas in the western Antarctic Peninsula. Lower values also occur in the ice boundary region in the Ross Sea. Similar to the Arctic, the ε_V of the sea ice is close to 1. It is interesting to note that high values of ε_H close to 0.90 are found during the Antarctic summer, in the west Weddell Sea, coinciding with lower N_r. Larger ε_H is a striking difference from the values found in the Arctic during the boreal summer.

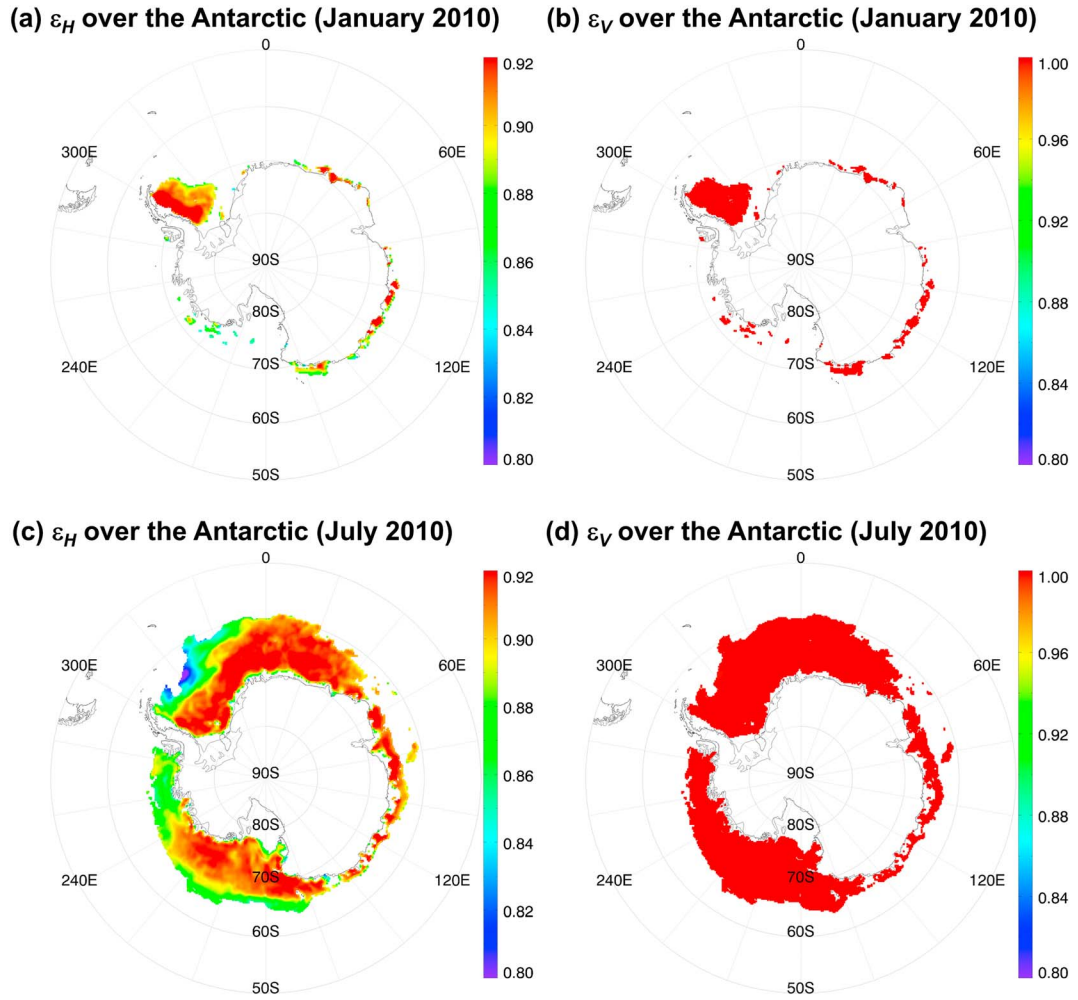

Figure 3. Same as in Figure 2 except for the Antarctic sea ice.

Using equations (5) and (6), ε_V at 6.9 GHz and 55° viewing angle were theoretically calculated using the refractive indices provided by *Sadiku* [1985] for pure ice, dry snow, and wet snow; the obtained values are 0.9995, 0.9999, and 0.9991, respectively. Therefore, the ε_V close to 1 found for both winter and summer months in both the Arctic and the Antarctic Oceans is consistent with the theoretically calculated values from pure ice, dry snow, and wet snow. The theoretically calculated ε_H are 0.7812, 0.9994, and 0.9792 for pure ice, dry snow, and wet snow, respectively. Although ε_H varies greatly from region to region and from season to season, retrieved ε_H values are between pure ice and dry (or wet) snow values.

The close agreement of the retrieved ε_V with the theoretically calculated ε_V for surface conditions (ice and/or snow) in the polar sea ice area strongly suggests that the proposed method is capable of retrieving surface emissivity at 6.9 GHz. However, since we lack available measurements of ε_H that varies greatly with the metamorphism of the emitting layer, it is difficult to evaluate the performance of the developed algorithm, except by indirectly examining the accuracy with theoretically expected values. In order to validate the algorithm indirectly, we compared the measured emissivity as a function of the satellite viewing angle with the theoretically calculated angular distribution of emissivity for various surface types.

Although AMSR-E only sees the target with a 55° viewing angle, retrieval of emissivity varying with viewing angle for one target (i.e., viewing the same target under different angles) is still possible because N_r from AMSR-E measurements should be independent of the viewing angle. Angularly varying emissivity can be calculated by inserting the retrieved N_r into equations (5) and (6) with varying viewing angles. The geographical distributions of obtained emissivity for nine viewing angles (0, 10, 20, 30, 40, 50, 60, 70, and 80°)

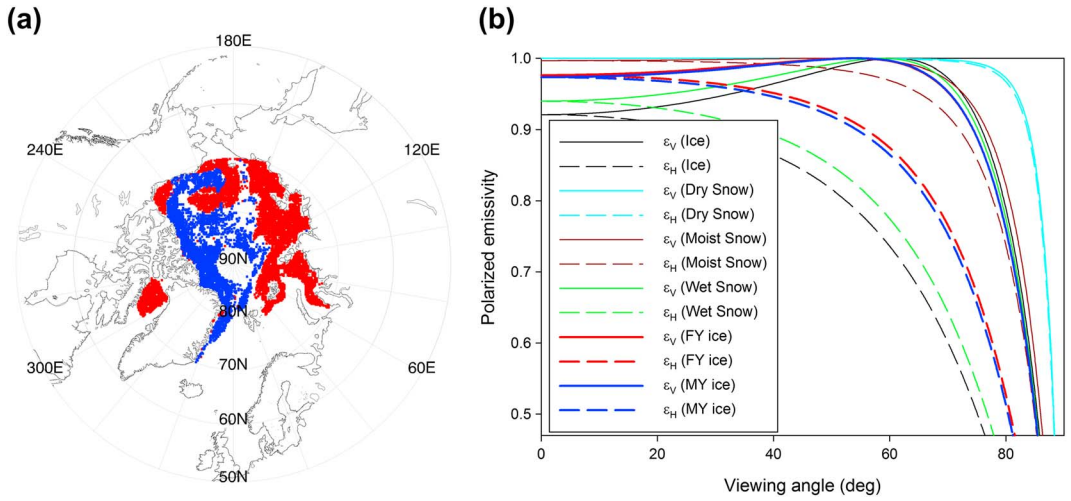

Figure 4. (a) Selected first-year (FY) ice area (red area) and multiyear (MY) ice area (blue area). (b) Angular variation of emissivities for sea ice and different types of snow (calculated from *Sadiku*'s [1985] refractive index). The solid and dashed lines represent the vertically and horizontally polarized emissivities. The black, cyan, brown, and green colors represent the theoretically calculated emissivities for pure ice, dry snow, moist snow, and wet snow, respectively, and the thick red and blue lines represent the retrieved emissivities over FY sea ice and MY sea ice area, respectively.

are given in Text S1 (Figures S1 and S2) in the supporting information. Here we provide the angular distribution of the polarized emissivity at two selected regions north of 70°N (Figure 4a), which shows the areas of the first-year sea ice (red area) and multiyear sea ice (blue area). To differentiate first-year ice from multiyear sea ice, we use the information on the sea ice age obtained from the National Snow and Ice Data Center [*Anderson et al*., 2014].

The retrieved polarized emissivities with varying viewing angles at two regions are provided in Figure 4b, along with the theoretically calculated emissivity distributions for pure ice and dry, moist, and wet snow based on *Sadiku*'s [1985] refractive index data. The retrieved ε_V tends to increase up to 1 until the Brewster angle of approximately 60° and then drops rapidly with increasing viewing angle. It is noted that magnitudes are between dry/moist snow and wet snow/pure ice when the angle is smaller than the Brewster angle and become quite similar to the ones found for pure ice/wet snow as the angle increases. The retrieved ε_H gradually decreases with increasing viewing angle until the Brewster angle and then decreases rapidly. Overall, these changes are similar to those theoretically calculated for pure ice, wet snow, and moist snow with *Sadiku*'s [1985] data. Throughout the entire range of viewing angles, magnitudes are between dry/moist snow and wet snow/pure ice. Considering that the emitting layer of 6.9 GHz should include signals from a combined layer of snow and pure ice underneath, the obtained distribution of emissivity in terms of shape and magnitude suggests that the proposed method is sound for retrieving the polarized emissivity of sea ice.

It is also of interest to examine the emissivity difference between old ice and new ice. Nearly the same emissivity distribution is found for ε_V between multiyear sea ice and fresh ice despite a slightly smaller emissivity for multiyear ice if the angle is lower than ~40°. However, slightly larger ε_H is found for fresh ice throughout the entire range of viewing angles compared with multiyear ice. This feature is consistent with observations and modeling studies that show that the emissivity of multiyear sea ice is generally smaller than the emissivity of the first-year sea ice [*Troy et al*., 1981; *Svendsen et al*., 1983; *Mathew et al*., 2008].

4.3. Physical Temperature of Sea Ice

Since the emissivity is available, the sea ice temperature representing the surface emitting layer can be estimated using equations (2) and (3). The retrieved sea ice temperatures from AMSR-E 6.9 GHz brightness temperatures for the Arctic and the Antarctic regions are provided in Figure 5. The retrieved sea ice temperatures over the Arctic during January show a generally homogeneous distribution, except for the relatively warm temperatures found in the eastern North Pole region, Hudson Bay, and the Chuckchi Sea. During the summer, the ice temperatures are quite similar to winter, which may suggest that this may be due

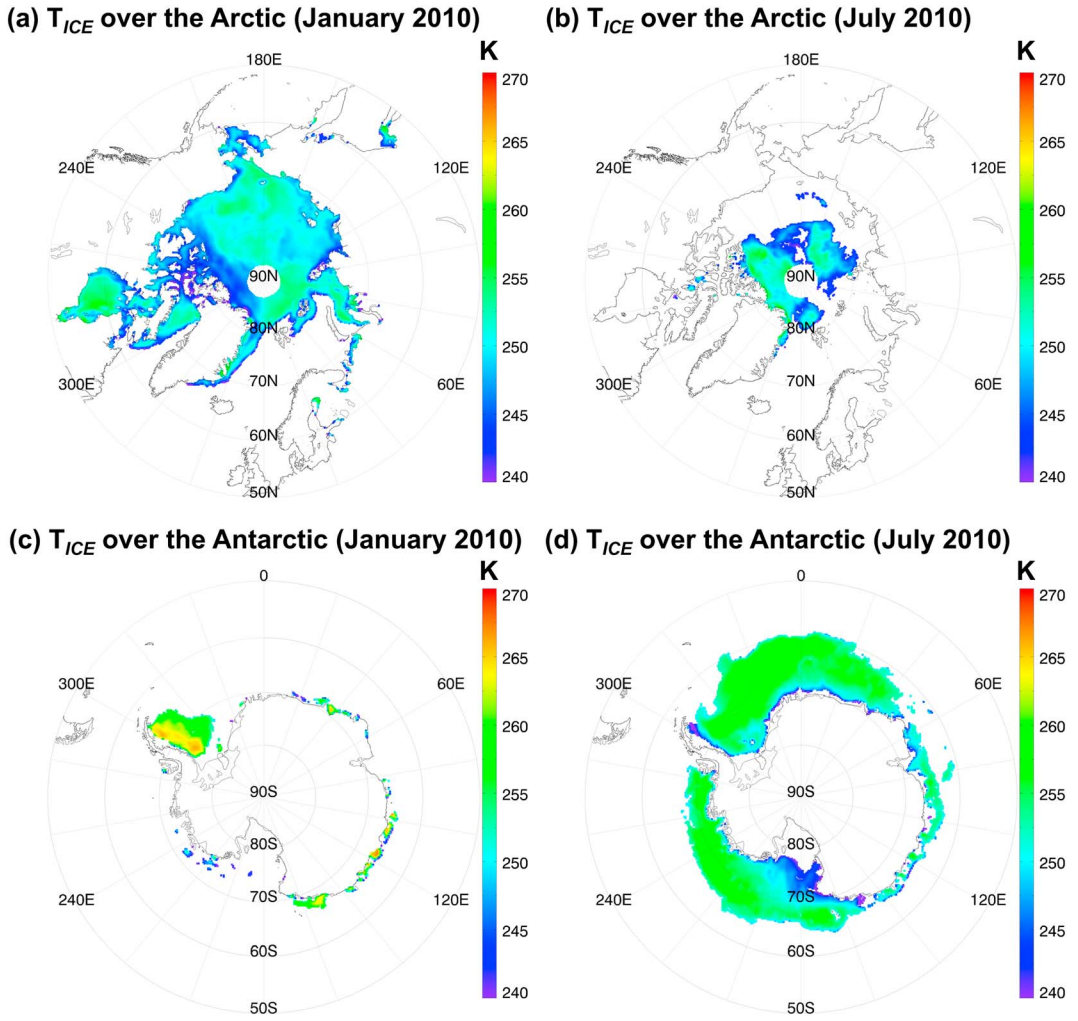

Figure 5. Same as in Figure 1 except for sea ice temperature.

to the open water contamination in the AMSR-E pixel size (43 km × 75 km). Since the emissivity of the open water is much lower than for ice or snow, this may invalidate the approximations of equations (2) and (3). The algorithm has been applied if sea ice concentration is larger than 95%. Cold temperatures over the Bering Sea during the winter also seem to be related to the open water contamination. Correction may be offered if the exact sea ice concentration is known; a possible correction method is discussed in Text S2 in the supporting information.

Antarctic sea ice temperatures are much warmer than for the Arctic, reaching up to approximately 260 K during the winter. Maximum temperature areas during winter are found in the northeast Weddell Sea and the area extending from the western Alexander Island to the Amundsen Sea. During the summer, temperatures reach close to 270 K, and the maximum temperature area is also found in the Weddell Sea.

The sea ice temperature over the Antarctic appears to be higher than that over the Arctic. It may be explained by the equatorward extent of the sea ice boundary in the Southern Hemisphere. The sea ice in the Southern Hemisphere further extends equatorward into the lower latitudes, compared to the Northern Hemisphere, probably causing the warmer sea ice temperature there. Also, the Southern Hemispheric ocean surrounding Antarctica should be considered, contrasting with the landmasses surrounding the Arctic Ocean.

Validating the proposed sea ice temperature retrieval algorithm, the derived sea ice temperature is compared with CRREL IMB data on a daily basis. In doing so, collocated data are constructed by the following steps: (1) Is the center point of any given AMSR 25 km × 25 km resolution target located within a 25 km distance from the IMB location? (2) Are sea ice concentrations from both ascending/descending brightness temperatures

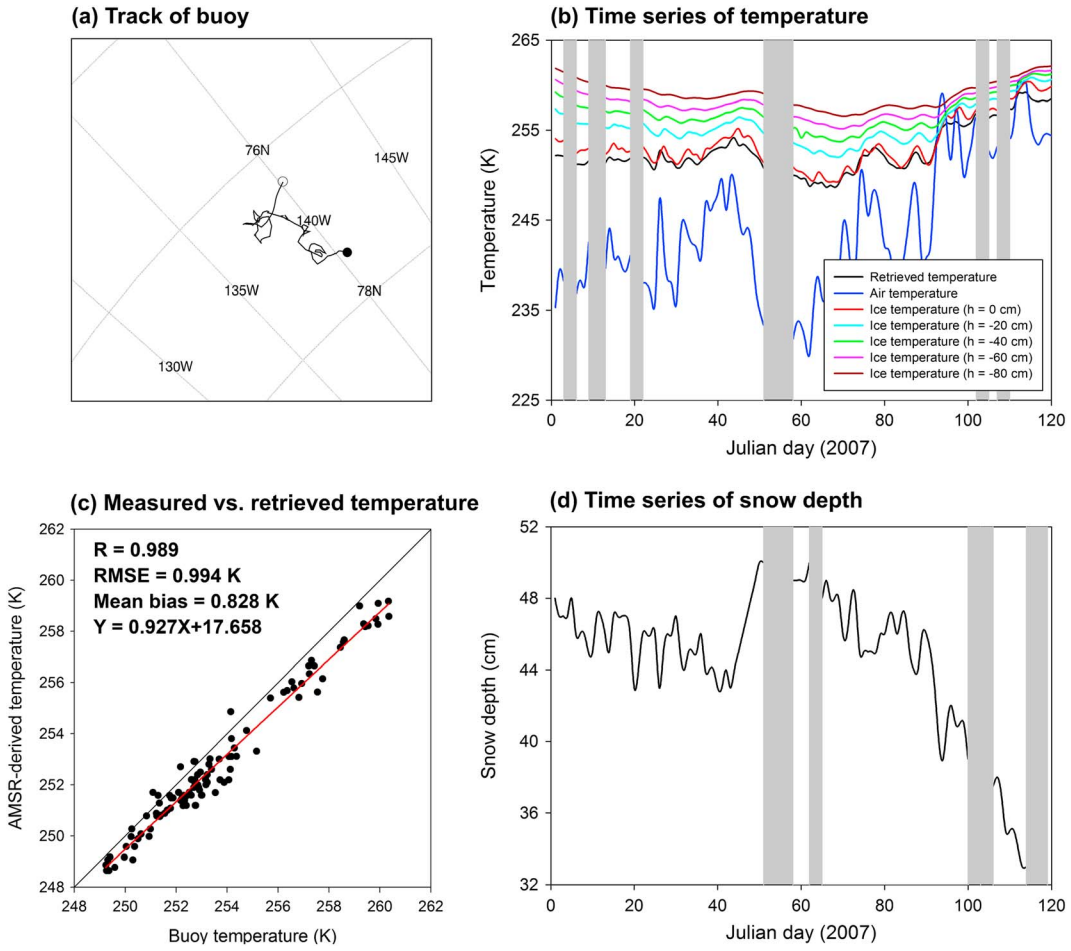

Figure 6. (a) CRREL drifting buoy track taken from 1 January 2007 (black dot: starting point, 77.44°N/140.39°W) to 30 April 2007 (open dot: ending point, 76.41°N/140.15°W); (b) time series of air temperature (blue), and temperatures of the ice at depth of 0 cm (red), −20 cm (cyan), −40 cm (green), −60 cm (pink), and −80 cm (dark red), and AMSR-retrieved ice temperature (black); (c) scatterplot of buoy-measured temperature at the ice depth of 0 cm versus AMSR-derived temperature with a regression line (red); and (d) time series of snow depth. The dates in Figures 6b and 6d are given in Julian day, and the gray bars represent data missing days.

greater than 98%? (3) Select the closest target from the buoy location if there are multiple targets satisfying the criteria of (2) and (3). CRREL IMB data collected along the drifting track (Figure 6a, from 1 January 2007 to 30 April 2007) were collocated with AMSR-derived ice temperatures after taking the selection procedures of (1)–(3). No target was selected after April because step (2) was not satisfied, and thus comparison is made until 30 April 2007.

Comparison results are presented in Figure 6. Here we correlate buoy-based point values with data representing averages over the fairly large target area of 25 km × 25 km within at most 25 km from the buoy location. Local surface conditions at the buoy location may not represent the satellite-employed large-pixel area because of horizontally varying sea ice thickness and snow depth/condition. Nevertheless, the time series of satellite-retrieved sea ice temperature resembles well the time series of buoy-measured sea ice temperature at the surface (i.e., $h = 0$ cm)—see Figure 6b, with a correlation coefficient of about 0.99 and a mean bias of 0.83 K (Figure 6c). The mean bias tends to become slightly larger with increasing temperature, in particular, during April, when the air temperature becomes far higher (Figure 6b) and the snow depth decreases rather quickly (Figure 6d). The larger bias may be in part due to the possible water-filled area within the target which can yield colder temperature, as discussed in Text S2 in the supporting information. It is interesting to note that the retrieved temperature appears to lead the temperature at $h = 0$ cm. It is because temperature signals come from a combined layer of snow and shallow upper layer of the ice underneath, as discussed in the surface emissivity and refractive index retrieval.

5. Conclusions and Discussion

In this study, we developed a new algorithm for retrieving physical properties of sea ice over the Arctic and Antarctic polar regions (i.e., the refractive index, polarized emissivities, and sea ice physical temperature) from AMSR-E 6.9 GHz brightness temperature measurements. The algorithm is based on the use of the analytical relationship between Fresnel-polarized reflectivities, practically not requiring a priori information in the MW remote sensing of sea ice parameters. As a case of reference, we selected 2 months representing winter and summer in both poles (i.e., January 2010 and July 2010) and used gridded monthly mean AMSR-E brightness temperature at 25 km × 25 km resolution. Also conducted was the validation of retrieved daily sea ice temperature using CRREL IMB measurements in the period from 1 January to 30 April 2007.

In order to avoid atmospheric influences in relating satellite-altitude measurements to surface properties, our analysis used low-frequency 6.9 GHz measurements. The retrieved refractive index and polarized emissivity of sea ice over both the Arctic and Antarctic regions and during summer and winter months are consistent with theoretical expected values calculated from refractive indices for various ice/snow surface conditions. It was demonstrated that the retrieved vertically polarized emissivity is found to be close to 1 regardless of region or season (Figures 2 and 3). Since the horizontally polarized component of the emissivity is now determined by $\varepsilon_H/\varepsilon_V = T_H/T_V$, the resultant ε_H should have the same degree of accuracy as ε_V, if brightness temperature measurements are correct. The close agreement of retrieved ε_V with theoretically expected values at the Brewster angle strongly suggests that the same degree of accuracy can be expected from ε_H. An alternative approach of using $\varepsilon_V/\varepsilon_H = T_V/T_H$ leads to a similar conclusion regarding the degree of accuracy of retrieved polarized emissivity.

The close agreement of retrieved sea ice temperature with CRREL IMB-measured ice temperature at the sea ice surface strongly suggests that the proposed retrieval algorithms of refractive index, polarized emissivity, and sea ice temperature are sound. It is because they are a single problem interlinked through the combined Fresnel equation, as expressed in equations (4), (10), and (11). Thus, the consistency noted in the comparison of retrieved and theoretically calculated emissivities can be applied to that for the temperature retrieval. Likewise, the statistics found in the comparison of retrieved temperature with in situ measurements can also be applied to that for the refractive index and polarized emissivity retrievals.

One caveat for sea ice temperature retrieval exists over the sea ice area mixed with open water, particularly in the marginal ice zone where the area is not entirely covered by ice. The problem seems to exist regardless of season. The simplified radiative transfer equations given in equations (2) and (3) may not work for open water without the atmospheric correction including the reflected upward flux. Even if the reflected upwelling radiance is negligible for the retrieval over snow/ice surface, it cannot be ignored over the open ocean because the emitting signal itself is small due to low emissivity. Therefore, any noise (or error induced by approximation) cannot be ignored over open water. Solving the full radiative transfer equation, with specified atmospheric condition and sea ice concentration, may offer a way to improve the algorithm.

Acknowledgments

The authors would like to thank three anonymous reviewers for their constructive and valuable comments, which led to deeper understanding of the retrieval problem. We acknowledge that AMSR-E data were from the Global Change Observation Mission data center (http://gcom-w1.jaxa.jp/); sea ice characterization data were obtained from the National Snow and Ice Data Center (NSIDC) (http://nsdic.org/); and CRREL IMB data were from the U.S. Army CRREL website (http://imb.erdc.dren.mil/). This work was funded by the Korean Polar Research Institute under grant PD14010.

References

Ackerman, S. A. (1996), Global satellite observations of negative brightness temperature differences between 11 and 6.7 μm, *J. Atmos. Sci.*, *53*(19), 2803–2812.

Anderson, M., A. C. Bliss, and M. Tschudi (2014), *MEaSUREs Arctic Sea Ice Characterization Daily 25 km EASE-Grid 2.0.*, NASA DAAC at the Natl. Snow and Ice Data Cent., Boulder, Colo., doi:10.5067/MEASURES/CRYOSPHERE/nsidc-0532.001.

Bromwich, D. H., et al. (2012), Tropospheric clouds in Antarctica, *Rev. Geophys.*, *50*, RG1004, doi:10.1029/2011RG000363.

Cavalieri, D. J., T. Markus, D. K. Hall, A. J. Gasiewski, M. Klein, and A. Ivanoff (2006), Assessment of EOS Aqua AMSR-E Arctic sea ice concentrations using Landsat-7 and airborne microwave imagery, *IEEE Trans. Geosci. Remote Sens.*, *44*(11), 3057–3069, doi:10.1109/TGRS.2006.878445.

Chassignet, E. P., and J. Verron (Eds.) (2006), *Ocean Weather Forecasting: An Integrated View of Oceanography*, pp. 577, Springer, Dordrecht, Netherlands.

Choudhury, B. J., T. J. Schmugge, A. Chang, and R. W. Newton (1979), Effect of surface roughness on the microwave emission from soils, *J. Geophys. Res.*, *84*(C9), 5699–5706, doi:10.1029/JC084iC09p05699.

Comiso, J. C. (1983), Sea ice effective microwave emissivities from satellite passive microwave and infrared observations, *J. Geophys. Res.*, *88*(C12), 7686–7704, doi:10.1029/JC088iC12p07686.

Comiso, J. C., D. J. Cavalieri, C. L. Parkinson, and P. Gloersen (1997), Passive microwave algorithms for sea ice concentration: A comparison of two techniques, *Remote Sens. Env.*, *60*(3), 357–384.

Comiso, J. C., D. J. Cavalieri, and T. Markus (2003), Sea ice concentration, ice temperature, and snow depth using AMSR-E data, *IEEE Trans. Geosci. Remote Sens.*, *41*(2), 243–252, doi:10.1109/TGRS.2002.808317.

De Jeu, R. A. M. (2003), Retrieval of land surface parameters using passive microwave remote sensing, PhD thesis, Dep. of Geo-Environ. Sci., Vrije Univ., Amsterdam.

English, S. J., and T. J. Hewison (1998), A fast generic millimeter-wave emissivity model, in *Microwave Remote Sensing of the Atmosphere and Environment*, *Proc. SPIE*, vol. 3503, pp. 288–300, Beijing, doi:10.1117/12.319490.

Flanner, M. G., K. M. Shell, M. Barlage, D. K. Perovich, and M. A. Tschudi (2011), Radiative forcing and albedo feedback from the Northern Hemisphere cryosphere between 1979 and 2008, *Nat. Geosci.*, *4*, 151–155, doi:10.1038/NGEO1062.

Girard, M.-C., and C.-M. Girard (2003), *Processing of Remote Sensing Data*, A. A. Balkema, Netherlands.

Gloersen, P., W. J. Campbell, D. J. Cavalieri, J. C. Comiso, C. L. Parkinson, and H. J. Zwally (1992), *Arctic and Antarctic Sea Ice, 1978–1987: Satellite Passive-Microwave Observations and Analysis*, *NASA SP-511*, 290 pp., National Aeronautics and Space Administration, Washington, D. C.

Haggerty, J. A., and J. A. Curry (2001), Variability of sea ice emissivity estimated from airborne passive microwave measurements during FIRE SHEBA, *J. Geophys. Res.*, *106*(D14), 15,265–15,277, doi:10.1029/2009JD900485.

Hall, D. K., J. R. Key, K. A. Casey, G. A. Riggs, and D. J. Cavalieri (2004), Sea ice surface temperature product from MODIS, *IEEE Trans. Geosci. Remote Sens.*, *42*(5), 1076–1087, doi:10.1109/TGRS.2004.825587.

Hewison, T. J., and S. J. English (1999), Airborne retrievals of snow and ice surface emissivity at millimeter wavelengths, *IEEE Trans. Geosci. Remote Sens.*, *37*(4), 1871–1879, doi:10.1109/36.774700.

Hwang, B. J., and D. G. Barber (2008), On the impact of ice emissivity on sea ice temperature retrieval using passive microwave radiance data, *IEEE Geosci. Remote Sens. Lett.*, *5*(3), 448–452, doi:10.1109/LGRS.2008.917266.

Hwang, B. J., J. K. Ehn, and D. G. Barber (2008), Impact of ice temperature on microwave emissivity of thin newly formed sea ice, *J. Geophys. Res.*, *113*, C02021, doi:10.1029/2006JC003930.

Kawanishi, T., T. Sezai, Y. Ito, K. Imaoka, T. Takeshima, Y. Ishido, A. Shibata, M. Miura, H. Inahata, and R. W. Spencer (2003), The advanced microwave scanning radiometer for the earth observing system (AMSR-E), NASDA's contribution to the EOS for global energy and water cycle studies, *IEEE Trans. Geosci. Remote Sens.*, *41*(2), 184–194, doi:10.1109/TGRS.2002.808331.

Key, J. R., R. Mahoney, Y. Liu, P. Romanov, M. Tschudi, I. Appel, J. Maslanik, D. Baldwin, X. Wang, and P. Meade (2013), Snow and ice products from Suomi NPP VIIRS, *J. Geophys. Res. Atmos.*, *118*, 12,816–12,830, doi:10.1002/2013JD020459.

Li, L., E. G. Njoku, E. Im, P. S. Chang, and K. St. Germain (2004), A preliminary survey of radio-frequency interference over the U.S. in Aqua AMSR-E data, *IEEE Trans. Geosci. Remote Sens.*, *42*(2), 380–390, doi:10.1109/TGRS.2003.817195.

Liou, K. (2002), *An Introduction to Atmospheric Radiation*, 2nd ed., Academic Press, San Diego, Calif.

Liu, Y., J. R. Key, R. A. Frey, S. A. Ackerman, and W. P. Menzel (2004), Nighttime polar cloud detection with MODIS, *Remote Sens. Env.*, *92*, 181–194, doi:10.1016/j.rse.2004.06.004.

Mai, S., C. Wamser, and C. Kottmeier (1996), Geometric and aerodynamic roughness of sea ice, *Boundary Layer Meteorol.*, *77*(3–4), 233–248, doi:10.1007/BF00123526.

Manninen, A. T. (1997), Surface roughness of Baltic sea ice, *J. Geophys. Res.*, *102*(C1), 1119–1139, doi:10.1029/96JC02991.

Markus, T., and D. J. Cavalieri (2000), An enhancement of the NASA Team sea ice algorithm, *IEEE Trans. Geosci. Remote Sens.*, *38*(3), 1387–1398, doi:10.1109/36.843033.

Markus, T., D. J. Cavalieri, A. J. Gasiewski, M. Klein, J. A. Maslanik, D. C. Powell, B. B. Stankov, J. C. Stroeve, and M. Sturm (2006), Microwave signatures of snow on sea ice: Observations, *IEEE Trans. Geosci. Remote Sens.*, *44*(11), 3081–3090, doi:10.1109/TGRS.2006.883134.

Mathew, N., G. Heygster, C. Melsheimer, and L. Kaleschke (2008), Surface emissivity of Arctic sea ice at AMSU window frequencies, *IEEE Trans. Geosci. Remote Sens.*, *46*(8), 2298–2306, doi:10.1109/TGRS.2008.916630.

Mathew, N., G. Heygster, and C. Melsheimer (2009), Surface emissivity of the Arctic sea ice at AMSR-E frequencies, *IEEE Trans. Geosci. Remote Sens.*, *47*(12), 4115–4124, doi:10.1109/TGRS.2009.2023667.

Mätzler, C., and U. Wegmüller (1987), Dielectric properties of fresh-water ice at microwave frequencies, *J. Phys. D Appl. Phys.*, *20*, 1623–1630, doi:10.1088/0022-3727/20/12/013.

Njoku, E. G., T. J. Jackson, V. Lakshmi, T. K. Chan, and S. V. Nghiem (2003), Soil moisture retrieval from AMSR-E, *IEEE Trans. Geosci. Remote Sens.*, *41*(2), 215–229, doi:10.1109/TGRS.2002.808243.

Peng, G., W. M. Meier, D. J. Scott, and M. H. Savoie (2013), A long-term and reproducible passive microwave sea ice concentration data record for climate studies and monitoring, *Earth Syst. Sci. Data*, *5*, 311–318, doi:10.5194/essd-5-311-2013.

Polashenski, C., D. Perovich, J. Richter-Menge, and B. Elder (2011), Seasonal ice mass-balance buoys: Adapting tools to the changing Arctic, *Ann. Glaciol.*, *52*(57), 18–26, doi:10.3189/172756411795931516.

Rosenfeld, S., and N. C. Grody (2000), Metamorphic signature of snow revealed in SSM/I measurements, *IEEE Trans. Remote Sens.*, *38*(1), 53–63, doi:10.1109/36.823901.

Sadiku, M. N. O. (1985), Refractive index of snow at microwave frequencies, *Appl. Opt.*, *24*(4), 572–575.

Sohn, B. J., and S.-M. Lee (2013), Analytical relationship between polarized reflectivities on the specular surface, *Int. J. Remote Sens.*, *34*(7), 2368–2374, doi:10.1080/01431161.2012.744490.

Stocker, T. F., D. Qin, G.-K. Plattner, M. Tignor, S. K. Allen, J. Boschung, A. Nauels, Y. Xia, V. Bex, and P. M. Midgley (Eds.) (2013), *IPCC, 2013: Climate Change 2013: The Physical Science Basis. Contribution of Working Group I to the Fifth Assessment Report of the Intergovernmental Panel on Climate Change*, 1535 pp., Cambridge Univ. Press, Cambridge, U. K., and New York, doi:10.1017/CBO9781107415324.

Svendsen, E., K. Kloster, B. Farrelly, O. M. Johannessen, J. A. Johannessen, W. J. Campbell, P. Gloersen, D. Cavalieri, and C. Mätzler (1983), Norwegian remote sensing experiment: Evaluation of the Nimbus 7 scanning multichannel microwave radiometer for sea ice research, *J. Geophys. Res.*, *88*(C5), 2781–2791, doi:10.1029/JC088iC05p02781.

Troy, B. E., J. P. Hollinger, R. M. Lerner, and M. M. Wisler (1981), Measurement of the microwave properties of sea ice at 90 GHz and lower frequencies, *J. Geophys. Res.*, *86*(C5), 4283–4289, doi:10.1029/JC086iC05p04283.

Ulaby, F. T., R. K. Moore, and A. K. Fung (1984), *Microwave Remote Sensing: Active and Passive: Volume I: Microwave Remote Sensing: Fundamentals and Radiometry*, Artech House, Norwood, Mass.

Ulaby, F. T., R. K. Moore, and A. K. Fung (1986), *Microwave Remote Sensing: Active and Passive: Volume III: From Theory to Applications*, Artech House, Norwood, Mass.

Ulander, L. M. H., R. Johansson, and J. Askne (1992), C-band radar backscatter of Baltic sea ice: Theoretical predictions compared with calibrated SAR measurements, *Int. J. Remote Sens.*, *13*(13), 2447–2468, doi:10.1080/01431169208904281.

Warren, S. G., and R. E. Brandt (2008), Optical constants of ice from the ultraviolet to the microwave: A revised compilation, *J. Geophys. Res.*, *113*, D14220, doi:10.1029/2007JD009744.

Wen, X., C. Xue, and Q. Dong (2011), The Arctic sea ice surface roughness estimation and application, in *Proceeding of the Twenty-first (2011) International Offshore and Polar Engineering Conference*, Int. Soc. Offshore and Polar Eng, Maui, Hawaii.

Wu, S. T., and A. K. Fung (1972), A noncoherent model for microwave emissions and backscattering from the sea surface, *J. Geophys. Res.*, *77*(30), 5917–5929, doi:10.1029/JC077i030p05917.

Zhang, S., J. Zhao, K. Frey, and J. Su (2013), Dual-polarized ratio algorithm for retrieving Arctic sea ice concentration from passive microwave brightness temperature, *J. Oceanogr.*, *69*, 215–227, doi:10.1007/s10872-012-0167-z.